Tribol Lett (2008) 31:177–185
DOI 10.1007/s11249-008-9350-1

ORIGINAL PAPER

Micro-to-Nano Indentation and Scratch Hardness in the Ni–Co System: Depth Dependence and Implications for Tribological Behavior

Sérgio Graça · Rogério Colaço · Rui Vilar

Received: 14 July 2008 / Accepted: 31 July 2008 / Published online: 12 August 2008

Abstract Although size effects in hardness have been extensively reported and analyzed for the static (indentation) case, much less attention has been given to these effects in non-static (scratch) hardness measurements. In the present work, size effects in the indentation and scratch hardness response of the Ni–Co system are evaluated by performing tests at several penetration depths, from the micro to the nanometer range. It is shown that, for all the range of compositions, the hardness response of these materials is strongly affected by the depth of penetration of the indenter: when the depth decreases, both the indentation and scratch hardness increase several times. This result denotes that, when studying the wear behavior of materials, special care must be taken concerning the scale one is dealing with, since the tribo-mechanical response of the material may change significantly from the micrometric to the nanometric contact scale.

Keywords Indentation · Scratching · Hardness · Size effect · Ni–Co system

1 Introduction

While the macrotribological behavior of rubbing components has been extensively studied for several decades, the study of the tribological response at the submicrometric contact scale (nanotribology) is a relatively recent research topic. Nanotribology has been largely stimulated by the advent of micro and nanotechnologies and by the invention of the atomic force microscope (AFM), which provided the ability of quantitative testing and observation of surfaces down to the quasi-atomic scale. Although wear and adhesion problems in moving contact parts of micro and nanoelectromechanical systems (MEMS and NEMS, respectively) have been the driving force for nanotribological studies, more recently other research paradigms have appeared, and the interest of nanotribology has been extended to conventional systems. In fact, the contact between nominally flat surfaces, in dry or boundary lubrication conditions, frequent in engineering components, is initiated by the contact between surface asperities whose contact areas can be of only a few tens of square nanometres (e.g. [1]). From this scenario it arises that the nanomechanical response of materials should be considered in the overall tribological evaluation of most systems.

It is of general acceptance that the hardness of a material is one of the most important properties controlling its wear resistance, a fact that arises from the qualitative definition of hardness as the "ability of a material to resist penetration or abrasion by other bodies" [2]. Therefore, in the models for both adhesive and abrasive wear of ductile materials (the most frequent forms of wear), the wear rate is inversely proportional to the indentation hardness. Concerning scratch hardness, the tests are in fact a form of controlled abrasive wear [3]. Consequently, it seems reasonable to use indentation or scratch hardness to rank materials for their likely resistance to wear, which has been done over the years (at least for a preliminary evaluation). However, the use of hardness, even for a preliminary evaluation of wear resistance, is not as straightforward as it could be expected since hardness is not an intrinsic property of the material. It depends on the type of indenter, mode of application (static, scratch, impact) and, moreover, on the magnitude of the applied load, which defines the penetration depth of the indenter.

S. Graça · R. Colaço (✉) · R. Vilar
Departamento de Engenharia de Materiais, Instituto Superior Técnico, Av. Rovisco Pais, 1049-001 Lisboa, Portugal
e-mail: rogerio.colaco@ist.utl.pt

Numerous studies have shown that, for submicrometric penetration depths, the indentation hardness of materials can differ significantly from that measured at macroscopic scales. In particular, it has been observed that shallow surface layers tend to exhibit a higher hardness than that of the bulk material (e.g. [4–7]). Therefore, the prediction of the wear behavior of a material made on the basis of macroscale hardness tests can be questionable in the nanometric range. This problem has recently called growing research interest, although it should be noted that Misra and Finnie [8] raised it, for the first time, long ago.

The motivation of this work is to evaluate the relation between metallurgical characteristics of metals and their hardness at various penetration depth scales, from the micro to the nanometer range. The Ni–Co system was chosen for this study because it is a known and well-characterized group of alloys: Ni and Co present almost complete miscibility in solid state, the stacking fault energy decreases linearly with increasing proportion of Co up to $\sim$70 wt.% [9] and, for compositions over $\sim$70 wt.% Co, a $\alpha \rightarrow \varepsilon'$ martensitic phase transformation can occur, thus leading to a steep variation of the bulk hardness of the material [10]. Moreover, this system is important from the tribological point of view, since Ni and Co are the main constituents of two of the most frequently used families of hardfacing alloys.

2 Experimental Methods

2.1 Materials Preparation

Ni + 9, 21, 26, 31, 42, 55, 73, 82, 85, and 92% Co, 100% Ni and 100% Co samples (all the compositions along the article are presented in weight proportion) were prepared in the form of thick coatings (thickness $\sim$1 mm) by powder injection laser cladding. The sample preparation procedure is described in detail elsewhere [11]. After laser processing, the surface of the coatings was ground with SiC abrasive papers (final grinding step with 4000 mesh paper) and polished with diamond particles suspensions (final polishing step with 0.1 μm diamond particles suspension), resulting in a final thickness of the coatings of $\sim$500 μm and a surface average roughness (R_a) smaller that 3 nm (measured by atomic force microscopy in 10 × 10 μm^2 areas, without using cut-off filtering).

2.2 Characterization Methods

After preparation, the phase constitution of the alloys was analyzed by X-ray diffraction (XRD) with a Siemens D5000 Bragg-Brentano diffractometer and CuK_α radiation ($\lambda_{average}$ = 1.5418 Å) and the samples were submitted to indentation and scratch hardness tests.

Vickers microindentation tests, with a load of 1 N and a 20 s hold time at maximum load, were performed with a Shimadzu HMV2000 apparatus. Vickers ultramicroindentation tests, with loads of 18 and 40 mN and a 30 s hold time at maximum load, were performed with a Fisherscope H100 displacement sensing apparatus. Nanoindentation tests, with a load of 57 μN, were performed with a DI Multimode Extended AFM, using a Veeco DNISP nanoindentation probe. The DNISP nanoindentation probe is a 3-sided diamond pyramid with tip apex angle of $\sim$93° and nominal tip radius of 40 nm, attached to a stainless steel cantilever with normal spring constant of 256 N/m (see Appendix for a detailed geometrical characterization). A procedure described in a previous publication [12] was adopted in order to minimize the influence of creep of the z-piezo scanner and of the lateral motion of the tip during the nanoindentation process.

Microscratch tests, with a load of 20 N, a scratching speed of 10 mm/min, and a scratch length of 10 mm, were performed with a CSEM Revtest apparatus and a Rockwell C indenter (diamond cone with included angle of 120°) with 100 μm tip radius. A Rodenstock RM600 optical profilometer was then used to retrieve the cross-section profiles of the grooves. Nanoscratch tests, with a load of 69 μN, a scratching speed of 3 μm/s, and a scratch length of 3 μm, were performed with the same AFM apparatus and indenter which were used in the nanoindentation tests. The micro and nanoscratches were always produced in the direction of the laser clad tracks. Since scratch hardness tests are non-static, the variation of the normal load during the movement of the indenter cannot be neglected. This variation was ±10 N in the conventional scratch tests and ±12 μN in the nanoscratch tests. The values of the width of the scratches were retrieved only from the central portion of the scratch to avoid the influence of start and stop effects.

Both the nanoindentations and nanoscratches were visualized in tapping mode using the DNISP probe, and the normal load applied by the cantilever in the nanoscale tests was calibrated by acquiring force curves in a rigid sapphire sample.

The results presented are an average of at least 10 measurements for each type of hardness test performed in each sample.

2.3 Hardness Calculations

The indentation hardness (H_i) of a material is given by:

$$H_i = \frac{F_N}{A_p}, \quad (1)$$

where F_N is the applied normal load and A_p is the projected area of the indentation. This definition of hardness was used to express the results of all indentation tests performed in

this work (Vickers hardness (H_V) can be related to the indentation hardness by $H_i = H_V/0.927$ [13]). In the case of ultramicroindentation tests, the indentation depth (contact depth) h was retrieved from the load-displacement curves and used to determine the projected area of the indentation by using the relation $A_p = 24.5h^2$ [14]. The projected area of nanoindentations was measured from the AFM images.

The scratch hardness (H_s) of a rigid-plastic material, retrieved from a scratch test performed with an indenter with certain geometry, is given by:

$$H_s = \eta \frac{F_N}{w^2}, \quad (2)$$

where F_N is the applied normal load, w is the width of the grove, and η is a geometrical constant. For a conical indenter η is $8/\pi$ [2], whereas for the DNISP geometry used in the nanoscratch tests its value is 4.786 (see Appendix for details). In this work it was assumed that, during the scratch test, the perimeter of the contact between the sliding indenter and the material is located at the surface mean line and, in this way, w is measured at the surface mean line. The width of microscratches was measured from the cross-section profiles obtained using optical profilometry, whereas the width of nanoscratches was measured from the AFM images.

In order to control image convolution effects, the nanoindentations and nanoscratches performed in some of the Ni–Co samples were visualized with sharp Si tips. It was concluded that convolution was within the experimental error.

3 Results

Figure 1a–g shows the XRD patterns of some of the analyzed Ni–Co alloys. As expected from the Ni–Co phase diagram [15], the microstructure of alloys within the compositional range up to 70% Co is formed only by the face centred cubic (FCC) α phase (Fig. 1a–d). The XRD pattern of the Ni–73%Co alloy (Fig. 1e) shows that this sample is formed by both α and the hexagonal close-packed (HCP) ε′ martensitic phase (in fact, the (200) peak is the only peak of α that is not overlapped by peaks of ε′). For Co contents larger than 80%, the samples are formed only by the ε′ phase (Fig. 1f, g).

Figure 2a and b shows the variation of indentation hardness in the Ni–Co system. It can be observed that the indentation hardness of all Ni–Co alloys increases significantly as the load decreases from the N to the μN range. Moreover, the hardness trend with alloy composition remains approximately independent of the load in the case of micro and ultramicroindentation, but changes slightly in the case of nanoindentation. In the micro- and

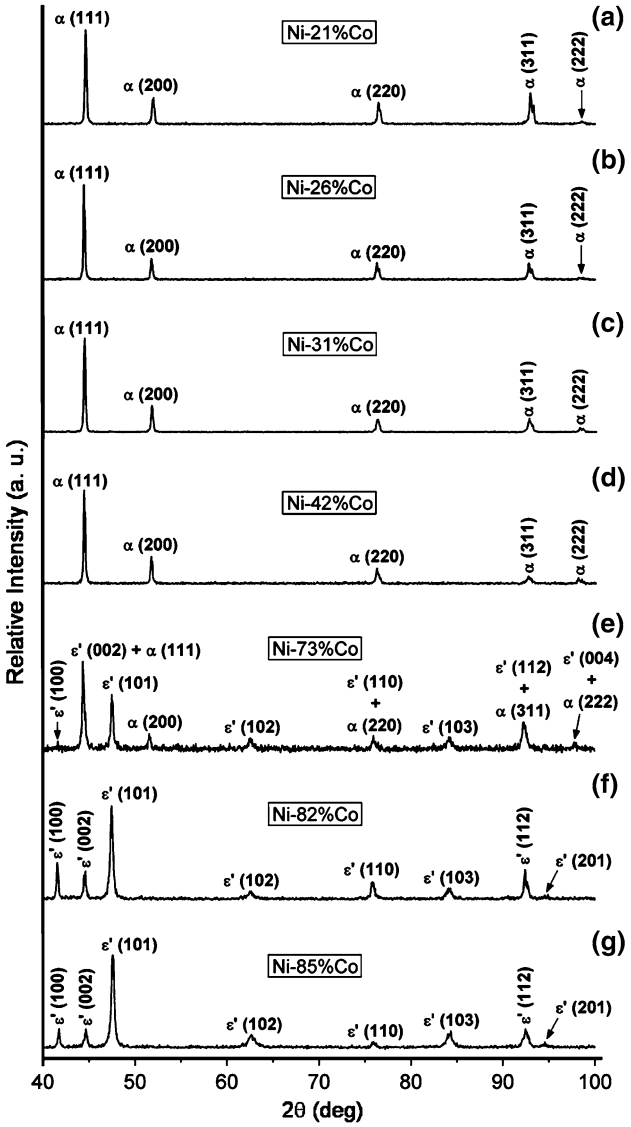

Fig. 1 X-ray diffractograms ($CuK_{\alpha 1}/CuK_{\alpha 2}$) of Ni–Co alloys with Co proportions in the range 21–85% (**a**–**g**)

ultramicroindentation tests (Fig. 2a), the hardness of the alloys tends to increase when the Co proportion increases from 9 to 35% and then decreases with increasing Co content from 35 to 55%. The exception in this compositional range is the composition Ni–26%Co, which presents lower hardness than the alloys in its vicinity, clearly visible in the ultramicroindentation results (Fig. 2a). For Co percentages larger than 70%, the hardness of the alloys increases again, with the maximum hardness value obtained at approximately 80% Co. The hardness values retrieved from nanoindentation tests (Fig. 2b), besides being substantially larger than those retrieved from ultra-micro and microindentation tests, present a more undefined tendency with increasing Co content and are more scattered. However, the higher hardness of Co-rich alloys and

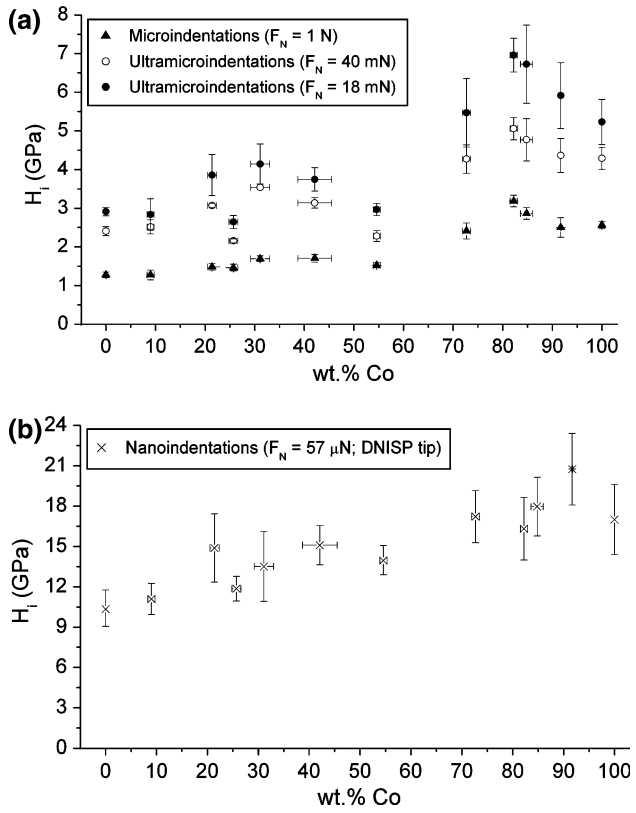

Fig. 2 Load (F_N) dependence of indentation hardness (H_i) in the Ni–Co system: (**a**) micro and ultramicroindentations; (**b**) nanoindentations

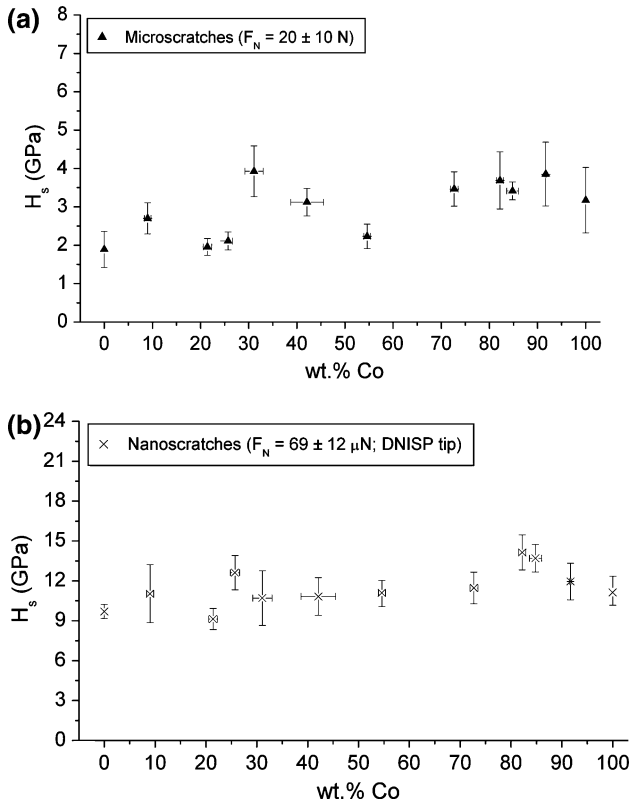

Fig. 3 Load (F_N) dependence of scratch hardness (H_s) in the Ni–Co system: (**a**) microscratches and (**b**) nanoscratches

the smaller hardness of the Ni–26%Co alloy can still be observed in Fig. 2b.

The scratch hardness values obtained from scratch tests performed with 20 N and 69 μN are depicted in Fig. 3a and b, respectively. Similarly to the case of indentation hardness, an increase of the scratch hardness with decreasing load is also observed for the entire range of Ni–Co alloys. The tendency of H_s with Co proportion is not as clearly defined as that of H_i in both micro and nanoscratch results. Nevertheless, despite the large scattering of results, a minimum of H_s in the range 21–26% Co, as well as the hardness increase for Co proportions over 70%, can be observed both in Fig. 3a and b.

In terms of absolute values, the indentation hardness is smaller than the scratch hardness when both are retrieved from tests performed with loads in the N range (Figs. 2a and 3a, respectively). In contrast, when hardness is retrieved from the nanoscale tests, in general, the indentation hardness is larger than the scratch hardness (Figs. 2b and 3b, respectively). This means that, while in microhardness tests the ratio H_s/H_i is larger than 1 ($1.16 < H_s/H_i < 2.32$), at the nanoscale this ratio is smaller ($0.58 < H_s/H_i < 1.06$). Consequently, the increase of hardness with decreasing contact scale is more pronounced in indentation than in scratching.

4 Discussion

In contrast to the considerable attention that has been dedicated to size effects in indentation, few works exist about size effects in scratch hardness. In the present work it is shown that size effects occur both in indentation and in scratch hardness and this result, together with the early unique observations of Gane and Skinner of scratch size effects in pure Au and Cu [16], strongly suggests that size effects occur not only in the static hardness response of metallic materials, but also in their response to non-static tests. Nevertheless, the differences between indentation and scratch hardness measurements prevent a direct comparison of the results and conclusions should be taken cautiously.

First of all, the differences between the measurement protocols for indentation and scratch hardness must be considered when comparing the results shown in Figs. 2 and 3. In scratch tests, the width of the grooves is measured at the surface mean line and not at the top of the ridges, while in the case of microindentation hardness, the length of the diagonals of the Vickers indentations is measured from optical observation from the top. Therefore, the measurement protocol in indentation corresponds approximately to the situation of measuring w at the top of the

scratch ridges. Consequently, this aspect leads to a trend of higher scratch hardness values as compared with indentation hardness ones. For example, the microscratch hardness of Ni and Co is 1.9 and 3.2 GPa, respectively, when w is measured at the surface mean line, and 1.4 and 2.4 GPa, respectively, when w is measured at the top of the ridges. These last values compare much better with the microindentation hardness of Ni and Co: 1.3 and 2.6 GPa, respectively. Secondly, scratch tests present an extra difficulty as compared to indentation ones, which consists of the fact that small inclinations of the surface of the sample relatively to the indenter sliding plane cause changes in the applied load during the tests. The influence of sample inclination can be observed by comparing the longitudinal cross-section profiles of nanoscratches performed in Ni (Fig. 4a, b) and Co (Fig. 4c, d). In both cases the load chosen was 57 μN and the scratches were performed from the lower to the higher region of the inclined surface. Due to sample inclination, in this example, the load increased from 57 to 61 μN in the nanoscratch test in Ni, while in the nanoscratch test in Co the load increased from 57 to 95 μN, which means that the Co sample has larger local inclination of the surface than the Ni one. Since the local inclinations of samples surfaces are impossible to eliminate and no load control loop is active during the scratch tests, the scratch hardness measurements are certainly affected by these variations of the normal applied load during the test. Even so, this latter error source leads, in general, to errors smaller than 10%, thus not affecting the trustworthiness of the scratch results if a statistically significant number of tests are performed. Nevertheless, it can lead to the smoothing of local steep variations of the hardness, which are more clearly detected in indentation hardness measurements.

Concerning the influence of alloy composition on hardness, it was observed that, as the penetration depth increases up to the micrometer range, both indentation and scratch hardness appear to be more sensitive to the composition of the alloys. The jump in the hardness values (both in indentation and scratch), occurring when the percentage of Co exceeds 70% Co (Figs. 2 and 3), can undoubtedly be attributed to the $\alpha \rightarrow \varepsilon'$ martensitic transformation, which is characteristic of the laser processed Co-rich alloys [10]. This is confirmed by the XRD results presented in Fig. 1f and g, which show that ε' predominates in the samples with more than 80% Co.

Also, a smooth increase of the hardness from approximately 20 to 35% Co followed by a decrease of the hardness until approximately 55% Co can be observed in both micro and ultramicro indentation and scratch tests (Figs. 2a and 3a, respectively). The exception to this trend are the alloys with compositions around 25% Co, which show a minimum of hardness, as compared to the other

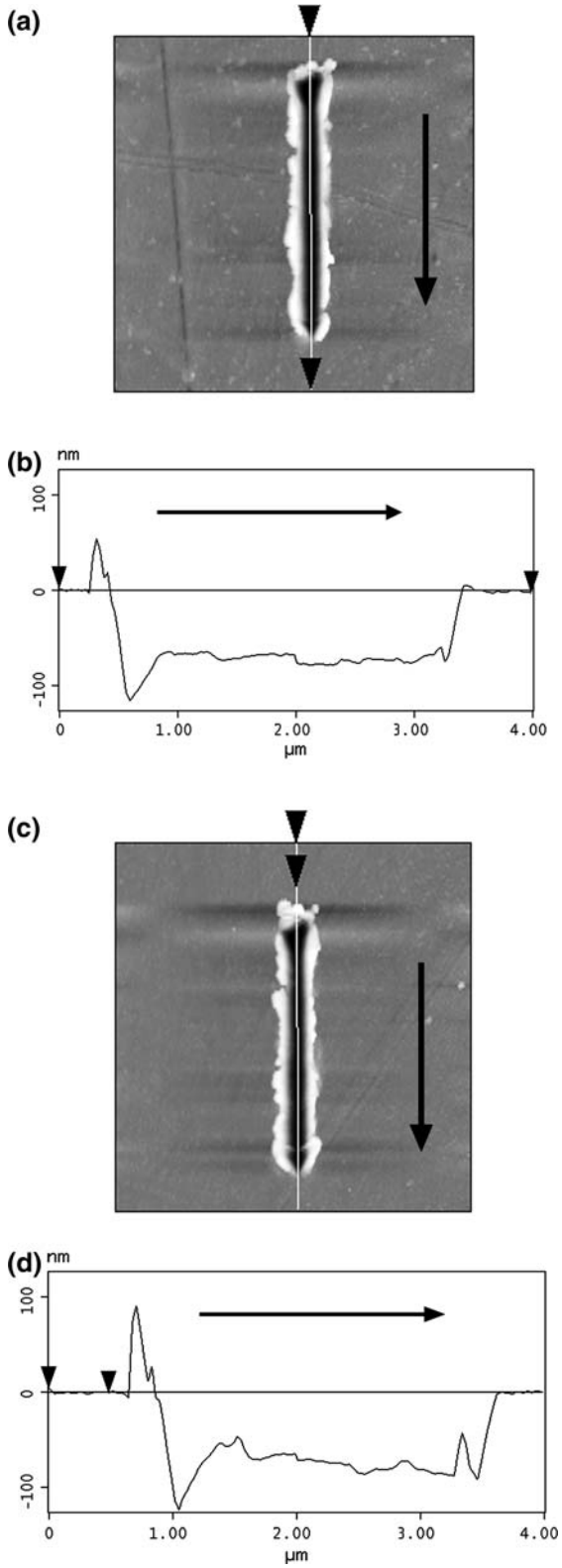

Fig. 4 AFM topographic image and longitudinal profile of nanoscratches performed in Ni (**a** and **b**, respectively) and Co (**c** and **d**, respectively). A Si tip was used to visualize the nanoscratches. The scratching direction is given by the black arrow in the figures

alloys in their compositional vicinity (Figs. 2 and 3). Although no evidence for differences in the microstructure can be found from the X-ray diffractogram of Fig. 1b (which can be expected due to the similarity of the X-ray scattering factors of Ni and Co atoms [17]), some authors [18, 19] have suggested that ordering may occur in Ni–25%Co, with the formation of a Ni_3Co superlattice. The presence of this phase is, however, quite controversial [20] and also it cannot explain, in a direct manner, the observed hardness decrease for the alloys in the compositional range around 25% Co. Nevertheless, the results presented in this article show clearly that there is an irregularity of the hardness trend in this short compositional range, which is observed, to a larger or smaller extent, in all the mechanical tests performed in this work.

The influence of contact scale in indentation and scratch hardness can be evaluated by comparing Figs. 2a and 3a with Figs. 2b and 3b, respectively. For penetration depths smaller than 100 nm (loads in the μN range), the composition-related trend of both indentation and scratch hardness is less clear than at larger contact scales, and the absolute values of hardness increase several times. This result shows that, at nanometric indentation depths, other factors besides composition and microstructure become increasingly relevant in the indentation and scratch response of the material. In a previous work [11], the authors have explained indentation size effects in Ni and Co with a model (recently validated by Ma et al. [21]) based on strain hardening effects and surface free energy.

Furthermore, it should be noted that the effect of native oxide layers on the hardness should not be neglected when the indentation depth is comparable to the oxide layer thickness [11]. In spite of the differences of the measurement protocols, which tend to lead to higher scratch hardness values, as mentioned earlier, the nanoindentation hardness values are higher than nanoscratch ones (Figs. 2b and 3b, respectively). This fact apparently confirms that the presence of thin native oxide films may have a non-negligible role on the material's hardness at nanometric contact scales. The depths of the nanoindentations and nanoscratches performed in Ni, Ni–55%Co, and Co are shown in Table 1. The experimentally measured depth of the nanoindentations is about 30 nm while that of nanoscratches is about 60 nm. The values found in the literature for the thickness of the native oxide layers in metals under environmental conditions are in the order of a few nanometers [22]. In this way, a possible explanation for the lower nanoscratch hardness as compared to nanoindentation hardness is the presence of nanometric native oxide layers, which have a stronger influence in static nanohardness tests than in non-static ones, due to the spalling of the thin oxide film during the scratch [23].

The results of this article show that the strength of small regions can be much higher than the bulk strength, i.e. the contact hardness under individual touching asperities can be considerably higher than that predicted from bulk measurements. Such effects might be of critical importance in the wear response of the material, either leading to a decrease of the wear coefficient as the penetration depth decreases or, as suggested by Gane and Skinner [16], to an increase of the size of the wear debris due to the breaking of cold welded junctions at regions distant from the original interface, which are weaker than the near interface regions. Therefore, the results presented here show that, if the contact scale during a tribological process is in the nanometer range (such as in finely polished surfaces submitted to average or low loads in dry or boundary lubrication conditions), macro and microhardness measurements, either indentation or scratch ones, can be of limited help for wear calculations or as a criteria for materials selection. Consequently, the tribo-mechanical characterization of materials at the nanoscale, either by nanoindentation, nanoscratch, or nanowear tests [24], should be considered in the evaluation of their wear resistance.

Table 1 Depth of nanoindentations (h_i) and nanoscratches (h_s) performed in Ni, Ni–55%Co, and Co, retrieved directly from the AFM images of nanoindentations and nanoscratches obtained with sharp Si tips

Sample	Nanoindentations		Nanoscratches	
	F_N (μN)	h_i (nm)	F_N (μN)[a]	h_s (nm)[a]
Ni	57	34 ± 3	59	64–78
Ni–55%Co	57	31 ± 3	64	61–76
Co	57	29 ± 3	76	64–87

[a] Average load

5 Conclusion

In the present work it was shown that size effects in hardness occur both in static (indentation) and non-static (scratch) hardness tests. The tested metallic system (Ni–Co), in all its compositional range, exhibits an increase of hardness when the penetration depth decreases from the micrometer to the nanometer range. This increase occurs both in indentation and in scratch hardness tests, and can go up to nine times in the former case and five times in the latter case. It is also shown that the trend with composition of both the indentation and scratch response of the material is less affected by the composition of the alloys in nanohardness tests than in microhardness ones, as it could be expected to some extent. These results stress the importance of the evaluation of surface mechanical properties at the nanoscale for an overall assessment of the tribological properties of materials.

Acknowledgments The authors thank Prof. Albano Cavaleiro for his help in performing ultramicrohardness experiments and FCT for the financial support of this research (Project Nanonico, POCTI/CTM/59376/2004). S. Graça also acknowledges FCT for the PhD grant SFRH/BD/17758/2004.

Appendix: Geometrical Characterization of Nanoindentation and Nanoscratch Hardness Tests

The Veeco DNISP diamond AFM tip used in this work is an equilateral triangular base pyramid (Fig. A1a) with tip apex angle of ~93° (Fig. A1b). Assuming that the tip is infinitely sharp (Fig. A2), the angle between the back face and the axis of the pyramid (β) is ~47.5°, while the angle between the front edge and the axis of the pyramid (α) is ~45.5°. By using simple trigonometric relations, the following equations can be obtained:

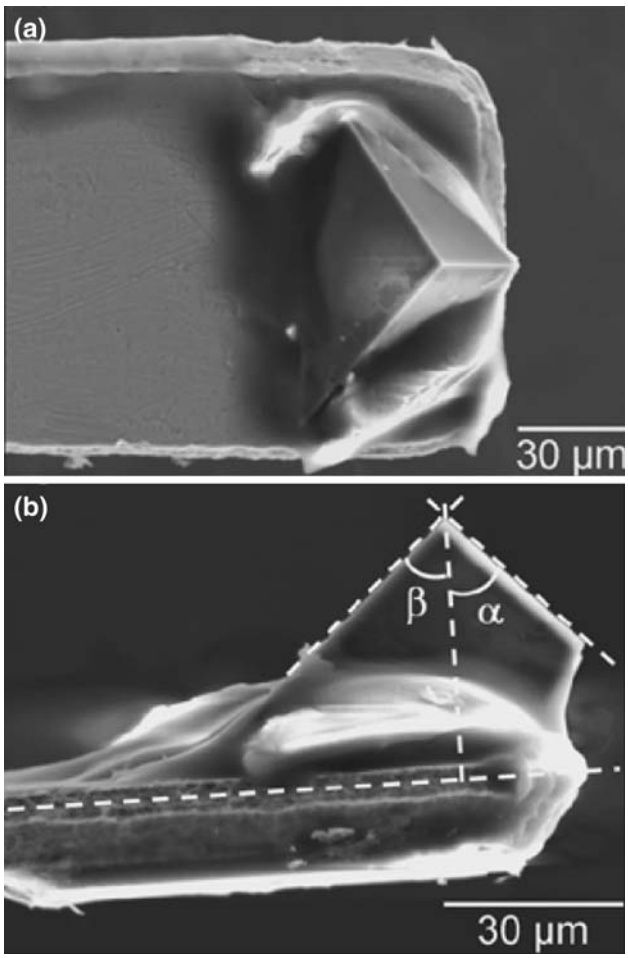

Fig. A1 SEM micrographs of Veeco DNISP probe viewed from bottom (**a**) and side (**b**). The side view shows that the top part of the diamond mounted on the cantilever is pyramidal, with the axis of the pyramid perpendicular to the cantilever, whereas the bottom part, where most of the glue is located, has irregular geometry

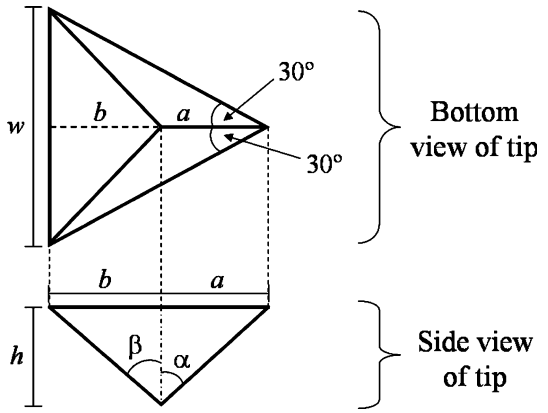

Fig. A2 Scheme of Veeco DNISP tip viewed from bottom (top) and side (bottom)

$$a = h\tan\alpha, \tag{A1}$$

$$b = h\tan\beta, \tag{A2}$$

$$w = \frac{a+b}{\cos 30}, \tag{A3}$$

with a, b, w, and h, defined in Fig. A2. Combining Eqs. A1–A3, the area function of the tip, $A_p(h)$, can be obtained:

$$A_p = \frac{w(a+b)}{2} = \frac{1}{\sqrt{3}}(\tan\alpha + \tan\beta)^2 h^2. \tag{A4}$$

Replacing the apex semi-angles α and β by the values retrieved from the SEM micrograph of Fig. A1b, an approximated value of the area function of the DNISP tip can be obtained:

$$A_p \approx 2.568h^2. \tag{A5}$$

A 2-D scheme of the DNISP tip scratching the surface of a material can be seen in Fig. A3. During the scratching process it is assumed that the perimeter of the contact is located at the surface mean line and, consequently, pile-up or sink-in effects do not contribute to the contact area. In this case w corresponds exactly to the width of the groove. Moreover, the contact between indenter and material only occurs at the two frontal faces of the pyramid (dark areas at the bottom part of Fig. A3). By introducing the values of a and b (given by Eqs. A1 and A2, respectively) in Eq. A3, and solving this equation in relation to h, the following relation is obtained:

$$h = \frac{\sqrt{3}w}{2(\tan\alpha + \tan\beta)}. \tag{A6}$$

From Fig. A3 results:

$$c = a\sin 30. \tag{A7}$$

Combining Eqs. A1, A6, and A7, c can be written as function of w:

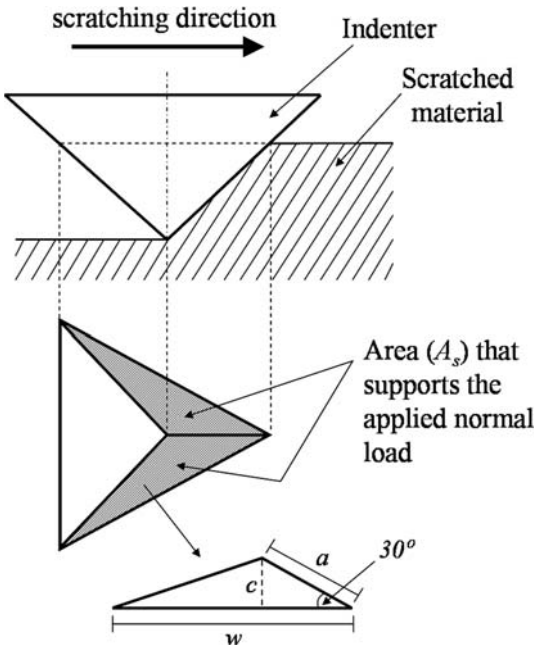

Fig. A3 Scheme of scratching process using the Veeco DNISP tip. The lateral view of the process and the bottom view of the indenter are shown, respectively, in the top and bottom parts of the figure

$$c = \frac{\sqrt{3}w}{4\left(1 + \frac{\tan\beta}{\tan\alpha}\right)}. \tag{A8}$$

The projected area of contact between indenter and material during the scratch test, A_s, is then given by:

$$A_s = 2\left(\frac{wc}{2}\right) = \frac{\sqrt{3}w^2}{4\left(1 + \frac{\tan\beta}{\tan\alpha}\right)}, \tag{A9}$$

and, finally, the scratch hardness (H_s) can be determined:

$$H_s = \frac{F_N}{A_s} = \eta\frac{F_N}{w^2}, \tag{A10}$$

with

$$\eta = \frac{4}{\sqrt{3}}\left(1 + \frac{\tan\beta}{\tan\alpha}\right). \tag{A11}$$

Replacing the apex semi-angles α and β by the values retrieved from the SEM micrograph of Fig. A1b leads to $\eta = 4.786$ for the DNISP tip.

The depth of the nanoindentations, h_i, can be estimated by combining Eqs. 1 and A5:

$$h_i \approx 0.624\sqrt{\frac{F_N}{H_i}}, \tag{A12}$$

where H_i is the indentation hardness measured from the AFM images of nanoindentations. The depth of the nanoscratches can be determined by combining Eqs. A6, A10, and A11 and replacing the apex semi-angles α and β by the values retrieved from the SEM micrograph of Fig. A1b:

$$h_s \approx 0.898\sqrt{\frac{F_N}{H_s}}, \tag{A13}$$

where H_s is the scratch hardness measured from the AFM images of nanoscratches.

References

1. Colaço, R.: Surface damage mechanisms from nano and micro-contacts to wear of materials. In: Meyer, E., Gnecco, E. (eds.) Fundamentals of Friction and Wear on the Nanoscale, pp. 453–480. Springer-Verlag (2007)
2. ASM handbook, vol. 18, Friction, Lubrication and Wear Technology. ASM International, Metals Parks, OH (1992)
3. Williams, J.A.: Analytical models of scratch hardness. Tribol. Int. **29**, 675–694 (1996). doi:10.1016/0301-679X(96)00014-X
4. Fleck, N.A., Muller, G.M., Ashby, M.F., Hutchinson, J.W.: Strain gradient plasticity – theory and experiment. Acta Metall. Mater. **42**, 475–487 (1994). doi:10.1016/0956-7151(94)90502-9
5. Ma, Q., Clarke, D.R.: Size dependent hardness of silver single-crystals. J. Mater. Res. **10**, 853–863 (1995). doi:10.1557/JMR.1995.0853
6. McElhaney, K.W., Vlassak, J.J., Nix, W.D.: Determination of indenter tip geometry and indentation contact area for depth-sensing indentation experiments. J. Mater. Res. **13**, 1300–1306 (1998). doi:10.1557/JMR.1998.0185
7. Liu, Y., Ngan, A.H.W.: Depth dependence of hardness in copper single crystals measured by nanoindentation. Scr. Mater. **44**, 237–241 (2001). doi:10.1016/S1359-6462(00)00598-4
8. Misra, A., Finnie, I.: On the size effect in abrasive and erosive wear. Wear **65**, 359–373 (1981). doi:10.1016/0043-1648(81)90062-4
9. Chaudhuri, D., Xie, D., Lakshmanan, A.N.: The influence of stacking fault energy on the wear resistance of nickel base alloys. Wear **209**, 140–152 (1997). doi:10.1016/S0043-1648(97)00010-0
10. Carvalho, P.A., Braz, N., Pontinha, M.M., Ferreira, M.G.S., Steen, W.M., Vilar, R., et al.: Automated workstation for variable composition laser cladding – its use for rapid alloy scanning. Surf. Coat. Technol. **72**, 62–70 (1995). doi:10.1016/0257-8972(94)02333-L
11. Graça, S., Colaço, R., Vilar, R.: Indentation size effect in nickel and cobalt laser clad coatings. Surf. Coat. Technol. **202**, 538–548 (2007). doi:10.1016/j.surfcoat.2007.06.031
12. Graça, S., Colaço, R., Vilar, R.: Using atomic force microscopy to retrieve nanomechanical surface properties of materials. Mater. Sci. Forum **514–516**, 1598–1602 (2006)
13. Tabor, D.: The Hardness of Metals. Oxford University Press, Oxford (2000)
14. Antunes, J.M., Cavaleiro, A., Menezes, L.F., Simões, M.I., Fernandes, J.V.: Ultra-microhardness testing procedure with Vickers indenter. Surf. Coat. Technol. **149**, 27–35 (2002). doi:10.1016/S0257-8972(01)01413-X
15. Metals Handbook, vol. 8, 8th edn. ASM, Metals Park, OH (1973)
16. Gane, N., Skinner, J.: Friction and scratch deformation of metals on a microscale. Wear **24**, 207–217 (1973). doi:10.1016/0043-1648(73)90233-0
17. Thompson, A.W.: Order in Ni 25 percent Co. Scr. Metall. **8**, 1167–1170 (1974). doi:10.1016/0036-9748(74)90489-X
18. Taylor, A.: Latice parameters of binary nickel cobalt alloys. J. Inst. Met. **77**, 585–594 (1950)

19. Garlipp, W., Cilense, M., Beatrice, C.R.S.: Evidence of short-range order in Ni-Co (25at-percent-Co) alloy by electrical-resistivity. Scr. Metall. Mater. **29**, 1035–1037 (1993). doi:10.1016/0956-716X(93)90173-P
20. Cable, J.W., Wollan, E.O., Koehler, W.C.: Distribution of magnetic moments in Pd-3D and Ni-3D alloys. Phys. Rev. **138**, A755 (1965). doi:10.1103/PhysRev.138.A755
21. Ma, Z., Long, S., Pan, Y., Zhou, Y.: Indentation depth dependence of the mechanical strength of Ni films. J. Appl. Phys. **103**, 043512 (2008). doi:10.1063/1.2885090
22. Mathieu, H.J., Datta, M., Landolt, D.: Thickness of natural oxide-films determined by AES and XPS with and without sputtering. J. Vac. Sci. Technol. A **3**, 331–335 (1985). doi:10.1116/1.573260
23. Thouless, M.D.: An analysis of spalling in the microscratch tests. Eng. Fract. Mech. **61**, 75–81 (1998). doi:10.1016/S0013-7944(98)00049-6
24. Degiampietro, K., Colaco, R.: Nanoabrasive wear induced by an AFM diamond tip on stainless steel. Wear **263**, 1579–1584 (2007). doi:10.1016/j.wear.2006.10.020